Hydrate Plugging and Flow Remediation during CO_2 Injection in Sediments

Jarand Gauteplass [1],* , Stian Almenningen [1] , Tanja Barth [2] and Geir Ersland [1]

[1] Department of Physics and Technology, University of Bergen, 5007 Bergen, Norway;
   stian.almenningen@uib.no (S.A.); geir.ersland@uib.no (G.E.)
[2] Department of Chemistry, University of Bergen, 5007 Bergen, Norway; Tanja.Barth@uib.no
* Correspondence: Jarand.Gauteplass@uib.no

Abstract: Successful geological sequestration of carbon depends strongly on reservoir seal integrity and storage capacity, including CO_2 injection efficiency. Formation of solid hydrates in the near-wellbore area during CO_2 injection can cause permeability impairment and, eventually, injectivity loss. In this study, flow remediation in hydrate-plugged sandstone was assessed as function of hydrate morphology and saturation. CO_2 and CH_4 hydrates formed consistently at elevated pressures and low temperatures, reflecting gas-invaded zones containing residual brine near the injection well. Flow remediation by methanol injection benefited from miscibility with water; the methanol solution contacted and dissociated CO_2 hydrates via liquid water channels. Injection of N_2 gas did not result in flow remediation of non-porous CO_2 and CH_4 hydrates, likely due to insufficient gas permeability. In contrast, N_2 as a thermodynamic inhibitor dissociated porous CH_4 hydrates at lower hydrate saturations (<0.48 frac.). Core-scale thermal stimulation proved to be the most efficient remediation method for near-zero permeability conditions. However, once thermal stimulation ended and pure CO_2 injection recommenced at hydrate-forming conditions, secondary hydrate formation occurred aggressively due to the memory effect. Field-specific remediation methods must be included in the well design to avoid key operational challenges during carbon injection and storage.

Keywords: CCS; carbon storage; injectivity; hydrate formation; flow remediation; CO_2; CH_4

1. Introduction

Carbon capture and storage (CCS) can contribute as a catalysator in the energy transition toward low-emission societies and reduced global warming. Captured CO_2 is proposed injected into depleted hydrocarbon reservoirs and saline aquifers for safe and permanent storage [1]. A high CO_2 injection rate is required to fully utilize the storage capacity and minimize project costs [2]. CO_2 injectivity can be compromised by salt and mineral precipitation [3–5], formation of biofilms [6], and formation of gas hydrates under favorable thermodynamic conditions [7,8]. This study highlights unwanted hydrate formation in sediments near the wellbore during subsurface CO_2 injection. Determining under which conditions the injectivity of a CO_2 well is impaired due to hydrate formation can lower the cost and risk barriers associated with carbon geo-sequestration.

Gas hydrates consist of hydrogen-bonded water molecules encaging guest molecules, such as CO_2 or CH_4, and form at moderate pressures and low temperatures. Formation of gas hydrates in porous media contributes to increased flow resistance and local blockage [9,10], which in turn leads to loss of injectivity near injection wells [11,12]. The degree of permeability reduction depends on the pore-level distribution of gas hydrates [13].

There can be significant differences in temperatures between flowing CO_2 in the injection well and the local geothermal temperature [14], possibly up to 50 °C difference [15]. Sudden changes in CO_2 injection rates affect the pressure in the near-well area almost instantaneously [16], and can agitate and accelerate hydrate nucleation under favorable thermodynamic conditions [17]. Large pressure drops (e.g., across a choke) can cause critical temperature reductions of the expanding CO_2 in terms of hydrate nucleation or dry ice formation. Local hydrate stable conditions can thus derive from cooling effects (e.g., Joule–Thomson) at depths normally outside the gas hydrate stability zone (GHSZ) [8,18–20]. CO_2 injection and storage in cold regions (e.g., Barents Sea) underlines the importance of CO_2 hydrate formation and dissociation kinetics in sediments.

Anthropogenic CO_2 injected into geological formations are likely to contain impurities, such as CH_4/N_2/amine residues [5,16,21], depending on the carbon capture technology applied. Impurities can alter thermodynamic properties and phase equilibria of the relevant fluids. Numerical simulations showed an extension of the GHSZ by almost 2 °C at 70 bar pore pressure if the CO_2 contained 5 mol% CH_4 [10]. CO_2 conditioning, e.g., by removing CH_4 residues from the CO_2 before injection and storage, can therefore lower the risk of subsurface hydrate formation. Also, dehydrating the CO_2 (<50 ppm H_2O) in the interface between CO_2 capture and transportation can eliminate the risk of hydrate formation and corrosion in pipelines, ships, and temporary surface storage containers [22]. However, in the subsurface near the injection well, flowing CO_2 is likely to be contacted by capillary backflow of formation water [3], facilitating availability of both guest and host (water) molecules required for hydrate formation.

Injection of anthropogenic CO_2 into existing gas hydrate reservoirs is a highly relevant method for solid carbon storage [23]. Here, binary gas injection can be a feasible injection strategy for CH_4–CO_2 exchange [24] and associated natural gas production. This has been demonstrated in a field test in Alaska, US, where unwanted reservoir fractures were avoided by mixing N_2 in the CO_2 injection column to reduce fluid weight [25]. In addition, initial injectivity reduction due to near-well hydrate formation was partially restored [26]. However, the high N_2 fraction (77 mol%) in the injection stream limited the overall volume of CO_2 stored. Other potential hydrate remediation methods are controlling the CO_2 temperature by heating the CO_2/wellbore [27]. Still, one major concern from localized heating is generation of system over-pressurization [28].

Thermodynamic inhibitors, such as methanol (MeOH) or ethylene glycol [29–31] and N_2 [28,32], are commonly used to dissociate gas hydrates by altering the hydrate phase equilibrium and destabilizing the hydrate structure at prevalent conditions. For example, N_2 purge has been reported to successfully dissociate porous CH_4 hydrates via growing channels in flow lines [28]. However, most hydrate dissociation studies have focused on CH_4 hydrate, as a means to produce natural gas resources stored as solid hydrates, or on hydrate avoidance in gas/oil pipelines, e.g., by adding low dosage hydrate inhibitors (LDHIs) in the stream [33]. While thermodynamic inhibitors shift the equilibrium of hydrate formation, LDHIs interfere and modify the hydrate crystal generation mechanisms. Unwanted CO_2 hydrate formation related to carbon geo-sequestration has not been thoroughly investigated, specifically in the near-wellbore region, where injected CO_2 interacts with surrounding sediments containing formation water and possibly native hydrates.

The main objective of this paper is to provide experimental insight into restoring CO_2 permeability after significant hydrate plugging in high-permeable sediments, to be used for validation of numerical flow models. Hydrate formation was assessed by parameters such as initial water saturation, solubility of guest molecule (CO_2 or CH_4) in water, and final hydrate saturation. Three common hydrate dissociation methods were investigated: N_2 injection, MeOH injection, and thermal stimulation. The limitation of using N_2 as a flow remediation method was linked to microfluidic observations. Finally, field implications of the observed data are discussed.

2. Materials and Methods

The core material consisted of Bentheimer sandstone (95.5% quartz, 2.0% kaolinite, 1.7% K-feldspar, 0.8% other [34]) with average measured porosity and absolute permeability of 22% and 1.1 D, respectively. The laboratory setup (Figure 1) facilitated logging of pressure drop (converted to normalized pressure gradient [bar/m] by distance corresponding to sample length), resistivity across the core sample, and upstream core surface temperature.
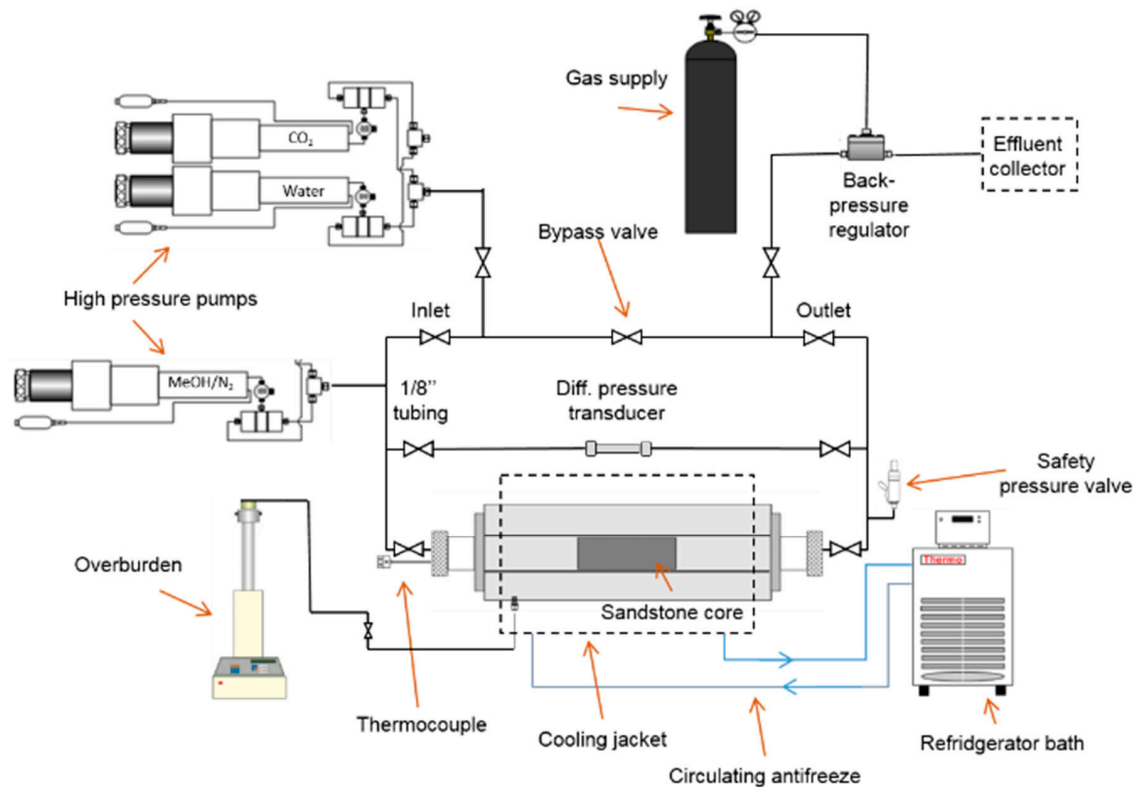

Figure 1. CO_2 core flow laboratory setup, including sandstone core sample (length ~15 cm), core holder, cooling system, pressure and temperature measurements, back-pressure regulator, and high-pressure pumps to regulate pore pressure and overburden. Modified from [10].

CO_2 hydrate: The core samples were pre-saturated with synthetic brine (3.5 wt% NaCl in distilled water) under vacuum. At 70 bar pore pressure, liquid CO_2 (99.999% purity) was injected at constant volumetric flow rate (0.5, 5.0, or 10.0 mL/min) into cooled (~4 °C), water-saturated sandstones. The low temperature was controlled by a refrigerator bath and maintained by circulating antifreeze through a cooling jacket that surrounded the core holder. Onset of hydrate formation within the pore space was determined from increased resistivity and flow resistance (pressure difference). Conducting three baseline experiments at corresponding flow rates outside the GHSZ ensured reference values of resistivity and permeability measurement where only saline water and liquid CO_2 occupied the pore space. After massive growth of CO_2 hydrates in the pore space, thermal stimulation or thermodynamic inhibitors (N_2, MeOH) were introduced to the system in an attempt to dissolve the hydrate plugs. The typical shut-in period from the end of CO_2 injection to the start of inhibitor injection was in most cases 15 min. Nitrogen was injected as compressed gas with purity of 99.6% N_2, whereas the methanol solution was composed of 30 wt% MeOH in distilled water; similar to concentrations used in previous dissociation studies [29–31]. The high-pressure pump delivering compressed N_2 or MeOH was connected to the flow system near the inlet side of the setup (see Figure 1). Thermal stimulation was conducted by increasing the set temperature of the refrigerator bath above the hydrate formation temperature and inducing gradual heating (0.3 °C/min) of the porous system.

CH$_4$ hydrate: The water-saturated core plug (spontaneous imbibition) was mounted into a rubber sleeve and placed inside a Hassler core holder. All flow lines leading into the core were purged under vacuum (except from the core plug itself) and filled with CH$_4$ gas. The CH$_4$ gas (>99.5%) was allowed to enter the core plug from both sides when the pressure in the flow lines reached atmospheric pressure, and the core plug was subsequently pressurized to 83 bar by a high-pressure pump. The confinement pressure was continuously kept at 30 bar above the pore pressure by applying pressurized oil around the rubber sleeve. The initially trapped air inside the core plug was assumed to dissolve as the CH$_4$ gas was pressurized to 83 bar. The core plug was pressurized at room temperature for approximately 24 h to allow CH$_4$ to dissolve in the water and to quantify the leakage rate of the system. Hydrate formation was initiated by decreasing the temperature of the core plug to ~0.5 °C. The pore pressure was maintained constant at 83 bar throughout the hydrate formation process, and the hydrate saturation was calculated by quantifying the amount of CH$_4$ gas that was consumed during hydrate growth [35]. A hydration number of 5.99 [36] was used to quantify the amount of water that was converted to CH$_4$ hydrate.

3. Experimental Results

Solid flow barriers developed from hydrate formation at constant injection rates (0.5, 5, and 10 mL/min) for CO$_2$ hydrates and static flow conditions for CH$_4$ hydrates. The induction time for flow-induced CO$_2$ hydrate formation ranged from approximately 0.5 PV to 2.5 PV (PV—pore volumes) of CO$_2$ injected under the same pressure and temperature conditions, demonstrating the stochastic nature of hydrate nucleation. Some injections showed signs of early hydrate formation followed by reduction in pressure gradient (re-opened gas channels) before final hydrate blockage and fully established flow barriers were formed. Pressure gradients of liquid CO$_2$ in the presence of hydrates exceeded 100 bar/m, and the injection was stopped as the pore pressure approached the confinement pressure. In contrast, CO$_2$ baseline flow experiments (0.5, 5, and 10 mL/min) outside the GHSZ measured a pressure gradient less than 1 bar/m on average.

N$_2$ injection: After massive hydrate growth and complete blockage of fluid flow, several relevant methods of remediation were tested. Figure 2 shows the pressure gradient development in Bentheimer sandstone during stages of CO$_2$ injection and subsequent N$_2$ injection, separated by a 15 min shut-in period. Cumulative volumes of CO$_2$ (triangles) and N$_2$ (circles) injected are displayed on the primary axis, and pressure gradient (squares) on the secondary axis. Hydrate formation within the pore space caused the pressure gradient to increase rapidly at around 30 min (2.2 PV) of CO$_2$ injection. Breakthrough of CO$_2$ occurred at 0.57 PV injected, and production of water/CO$_2$ was not observed after hydrates formed in the core sample (0.37 frac. initial water saturation). CO$_2$ injection was ended when the pressure gradient reached 130 bar/m. The following decay of the pressure gradient was directly linked to CO$_2$ consumption during continuous hydrate growth while the system no longer had pressure support. N$_2$ injection was initiated at 55 min, first at constant volumetric flow rate (1 mL/min), and later at constant pressure (90 bar), to keep the pressure gradient below 130 bar/m. A total of 40 mL N$_2$ was injected over a period of 175 min without any effect on the pressure gradient or observations of produced fluids from the core sample. N$_2$ injection failed to dissolve the CO$_2$ hydrate plug and restore injectivity within the given time frame.

N$_2$ was also used to infer the effective permeability in a core (0.65 frac. initial water saturation) sample after CH$_4$ hydrate formation. The core was saturated with 0.55, 0.22, and 0.23 (frac.) of CH$_4$ hydrate, water, and CH$_4$ gas, respectively, prior to N$_2$ injection. Figure 3 displays responses in pressure gradient (squares) and temperature (circles) of the sandstone sample with time. As N$_2$ was injected with constant volumetric rate equal to 2 mL/h, the pressure gradient (squares) built up rapidly to 55 bar/m (Figure 3), and maintained for 24 h after with no injection. The injection of N$_2$ was recommenced with identical injection rate until the pressure gradient reached approximately 90 bar/m. The injection was again stopped, and the core was isolated while maintaining continuous pressure readings at both inlet and outlet sides. No sign of hydrate dissociation was observed during

600 h. In fact, the pressure gradient increased slightly in this period, but this was attributed to a small leakage in the outlet flow line. Continued growth of CH_4 hydrates may also have contributed to the decreasing outlet pressure. Note that the average core temperature was only 0.5 °C during this experiment (Figure 3). The temperature was therefore bumped to 2.0 and then 2.8 °C while keeping the inlet pressure constant to 95 bar, to verify that the pore water was in liquid state and that there was no solid ice obstructing the flow of N_2. The pressure gradient dropped initially, due to thermal expansion of CH_4 gas at the outlet side, but the pressure gradient stabilized as the temperature stabilized and the core was still blocked. In contrast, a Bentheimer core experiment (0.63 frac. initial water saturation) with lower final CH_4 hydrate saturation (0.48 frac.), experienced successful hydrate dissociation by N_2 injection (30 mL). This is shown in Figure 4 by an abrupt reduction in differential pressure (squares) after approximately 500 h. On a later stage, binary gas injection was tested, first at 75/25 mol% ratio of N_2/CO_2 at constant rate of 1.2 mL/h (at 800 h), and finally at 50/50 mol% (at 900 h) without indications of hydrate reformation (differential pressure remained low while volume of N_2 injected increased steeply). A similar experiment conducted by this research group [24] demonstrated restored flow by N_2 injection in a CH_4 hydrate-plugged Bentheimer sandstone (~0.5 frac. initial water saturation). Here, final core saturation was 0.46, 0.29, and 0.25 (frac.) of CH_4 hydrate, water, and CH_4 gas, respectively, prior to N_2 injection and successful dissociation of the hydrate plug.
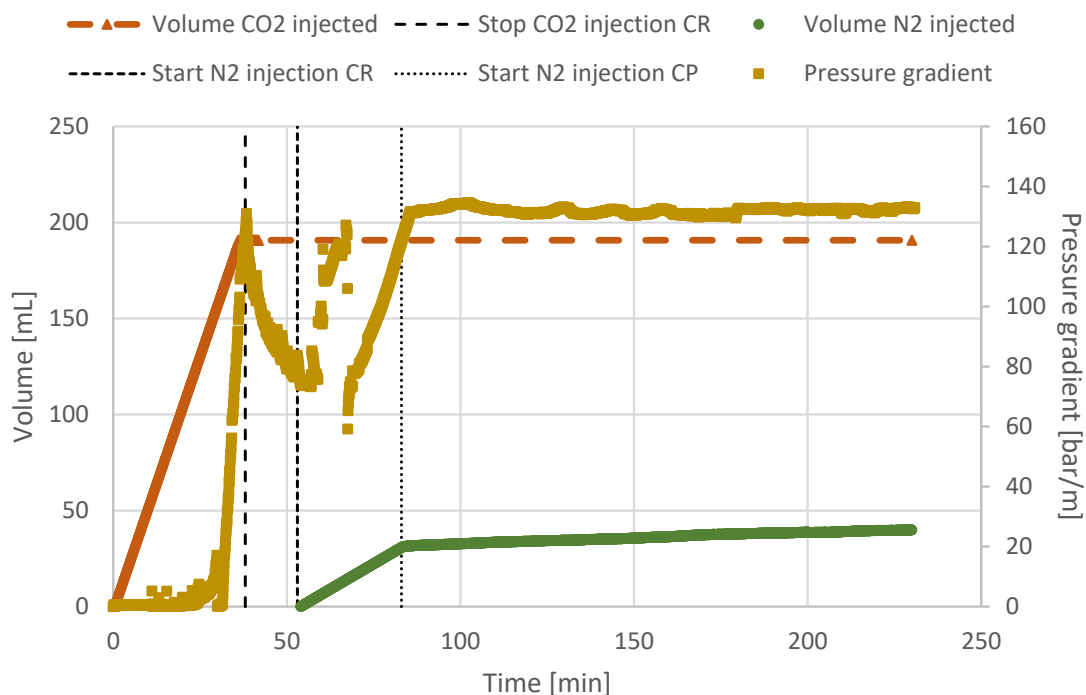

Figure 2. Cumulative volumes of CO_2 (triangles) and N_2 (circles) injected, and pressure gradient (squares) measured during flow-induced hydrate formation in sandstone (14.52 cm core length). CO_2 injection (5.0 mL/min) was followed by a 15 min shut-in period before the N_2 injection started (1.0 mL/min). Partial re-establishment of flow was observed at 67 min (sudden drop in inlet pressure), followed by gradual increase in pressure gradient due to continued hydrate growth. The N_2 injection was set to constant pressure injection (90 bar) when the pressure gradient exceeded 130 bar/m.
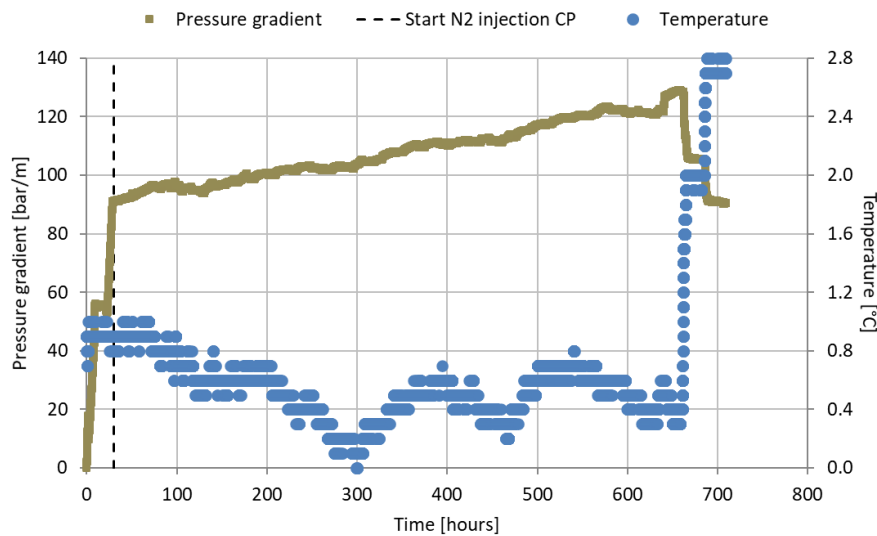
Figure 3. Pressure gradient (squares) profile during N_2 injection (start pressure control indicated by vertical broken line) into a sandstone core (14.94 cm length) saturated with 0.55 (frac.) of CH_4 hydrate, 0.22 (frac.) of water, and 0.23 (frac.) of CH_4 gas. The temperature (circles) was measured on the surface of the core-end at the outlet side.
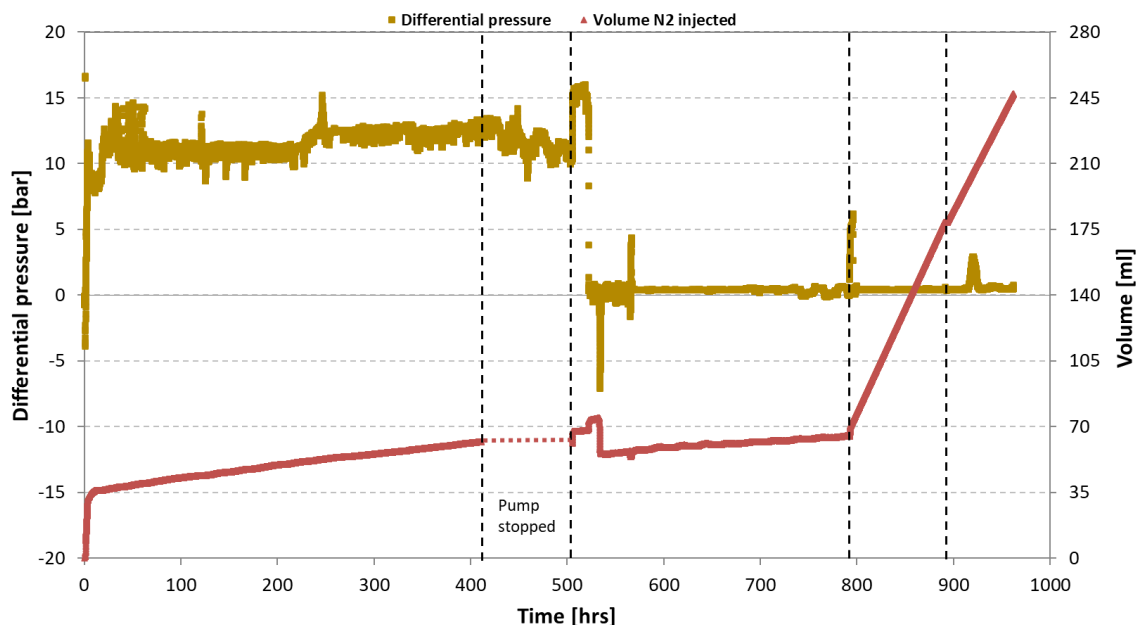

Figure 4. Differential pressure (squares) during N_2 injection into a sandstone core (14 cm length) saturated with 0.48 (frac.) of CH_4 hydrate, 0.24 (frac.) of water, and 0.28 (frac.) of CH_4 gas. Volume of N_2 injected (triangles) is displayed on the secondary y-axis. Binary gas injection of N_2/CO_2 is indicated with broken vertical lines at 800 h (75/25 mol%) and 900 h (50/50 mol%). Experimental conditions were $T = 4\ °C$, 3.5 wt% brine salinity, and pore pressure of 83 bar.

MeOH injection: Figure 5 shows CO_2 hydrate plug remediation by MeOH injection into a Bentheimer sandstone core (0.36 frac. initial water saturation). Volumes of CO_2 (triangles) were injected in four stages, accompanied by immediate response in the pressure gradient (squares) due to hydrate formation. Pausing the CO_2 injection caused the upstream pressure to decline because of liquid CO_2 being converted to solid hydrates, and restarting CO_2 injection led to rapid increase in pressure because of blocked flow paths. In order to restore injectivity in the core plug, a MeOH flush was initiated approximately 15 min after the last CO_2 restart. A total of 25 mL solution of 30 wt% MeOH

was injected over a period of 136 min before the hydrate plug dissociated and the injectivity was fully restored. During the CO_2 hydrate dissociation, the pressure gradient was reduced by 100 bar/m within 45 s. In contrast, pressure decline during hydrate growth without pressure support (e.g., at timestep 25 min) required around 25 min to obtain the same pressure gradient reduction.
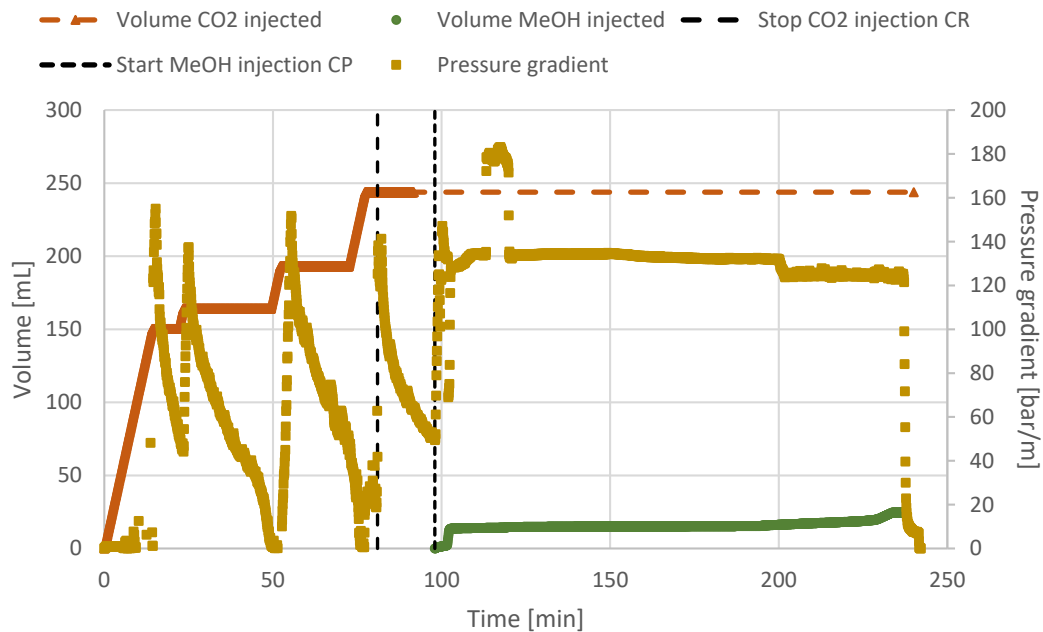

Figure 5. Cumulative volumes of CO_2 (triangles) and MeOH (circles) injected, and pressure gradient (squares) measured during flow-induced hydrate formation and dissociation (14.76 cm core length). Vertical broken lines indicate end of stages of CO_2 injection (10 mL/min), and start of MeOH injection (90 bar pressure control) after a shut-in period of approximately 15 min. A local pressure increase was measured at timestep 110 min, caused by temporarily reduced outlet pressure (not believed to have any effect on the outcome of the experiment).

Thermal stimulation: MeOH injection was combined with thermal stimulation in another Bentheimer core experiment (0.64 frac. initial water saturation). Figure 6 displays the development of pressure gradient (squares) and temperature (circles) through the stages of CO_2 hydrate formation and dissociation in the porous medium. The horizontal line indicates equilibrium temperature for CO_2 hydrate at initial pore pressure of 70 bar (PVTsim Nova 2). Above the line, the hydrate structure will destabilize and dissociate into liquid water and CO_2. A spike in temperature occurred after 68 min, accompanied by a steady increase in differential pressure, marking the exothermic onset of sedimentary hydrate growth. The CO_2 injection was ended after 190 min, reaching a pressure gradient of 127 bar/m. Hydrates continued to grow without pressure support during the 45-min-long shut-in, reducing the pressure gradient to approximately 15 bar/m. The following MeOH injection failed to contact the hydrate plug (total of 4 mL MeOH injected over 63 min), due to near-zero permeability. Consequently, thermal stimulation was used as a remediation method and the formation temperature was increased by 0.3 °C/min after 310 min of total run time. The pressure gradient declined by approximately 3 bar/m per minute while still in the predicted GHSZ (below 8.3 °C), due to initial lack of pressure support during additional hydrate growth, followed by outlet pressure increase due to thermal CO_2 expansion. When the formation temperature exceeded the GHSZ, the pressure gradient fell 70 bar/m in less than a minute, showing efficient decomposition of the CO_2 hydrates. After a full dissociation, the temperature was set to initial conditions (4 °C) at a cooling rate of 0.1 °C/min. Having restored the connectivity of the formation, a second CO_2 cycle was initiated at 383 min, inside the GHSZ (7.1 °C). This resulted in an instant secondary hydrate formation enhanced by the memory effect.
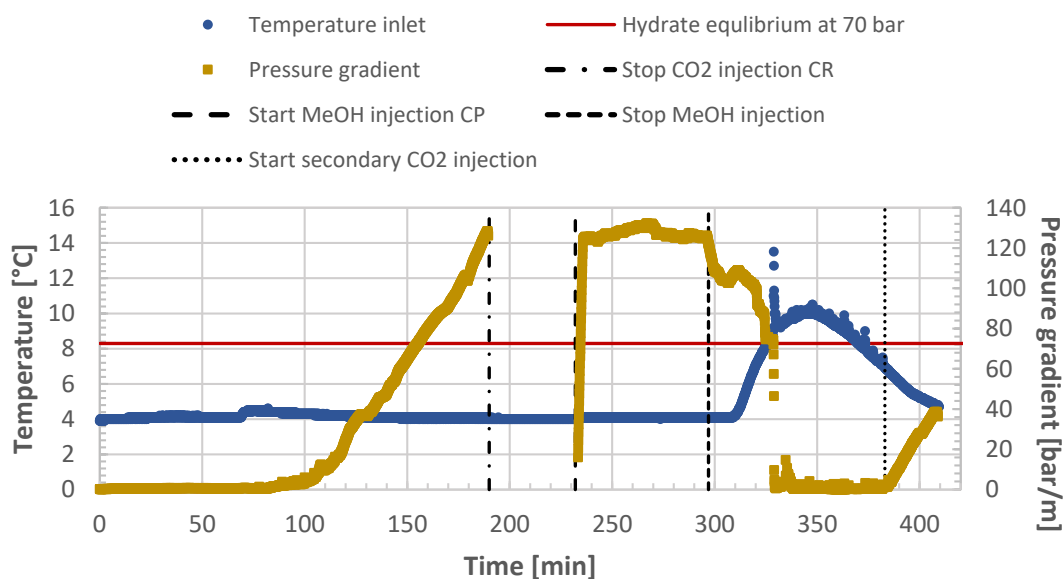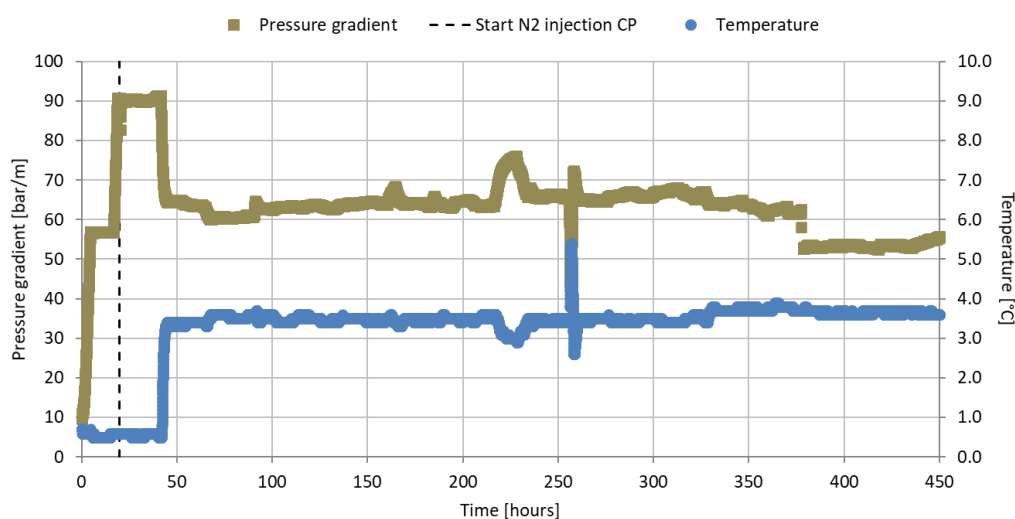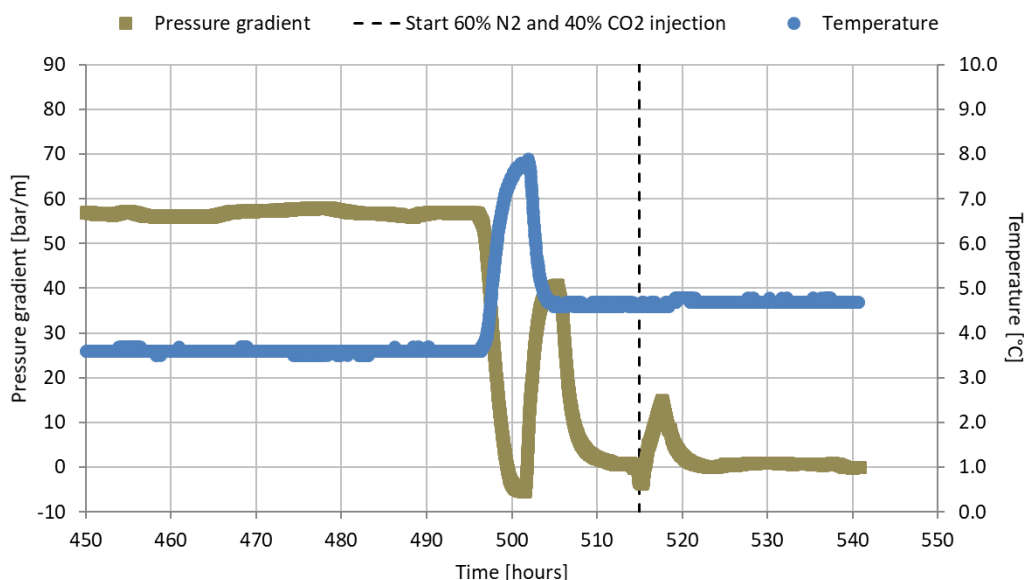
Figure 6. Temperature (circles) and pressure gradient (squares) measured during flow-induced hydrate formation and dissociation by thermal stimulation in sandstone sample (14.81 cm length). The temperature was regulated using the refrigerating fluid. The horizontal line indicates numerical estimate of equilibrium temperature for CO_2 hydrate at initial pore pressure of 70 bar. Vertical broken lines indicate end of CO_2 injection (0.5 mL/min), start and end of MeOH injection (85 bar pressure control) after a shut-in period of 45 min, and start of secondary CO_2 injection (0.5 mL/min).

N_2 injection was also combined with thermal stimulation to obtain injectivity in a core (0.69 frac. initial water saturation) of high final CH_4 hydrate saturation. The core was saturated with 0.61, 0.21, and 0.18 (frac.) of CH_4 hydrate, water, and CH_4 gas, respectively, prior to N_2 injection. Figure 7 displays responses in pressure gradient (squares) and temperature (circles) as functions of injection time. As N_2 was injected with constant volumetric rate equal to 4 mL/h, the pressure gradient built up rapidly to approximately 55 bar/m (Figure 7a). The injection was therefore halted for 24 h, but this did not result in any change in the pressure gradient. The injection of N_2 was restarted with identical injection rate until the pressure gradient reached approximately 90 bar/m. The injection scheme was then set to constant pressure delivery at 95 bar. The average temperature was initially low, at T = 0.7 °C, but it was eventually increased to T = 3.5 °C, to ensure no solid ice in the pore space. Consequently, the pressure gradient dropped to 60–70 bar/m because of thermal expansion of CH_4 gas at the outlet side (Figure 7a). Still, there was no sign of improved injectivity during a period of 400 h. The fluctuations in the pressure gradient followed the temperature fluctuations, and the small drop in the pressure gradient after 375 h was due to adjusting the constant pressure injection to 93 bar. The failure of N_2 injection to restore injectivity called for other flow remediation methods. The system temperature was therefore increased to T = 8 °C and down again to T ~4.5 °C, over a timespan of eight hours (Figure 7b). Within a few hours after the system temperature was stabilized at T ~4.5 °C, the pressure gradient dropped rapidly to zero, meaning that the outlet and inlet pressure equilibrated due to sedimentary hydrate dissociation. Because the theoretical equilibrium temperature was not reached in the experiment (~9.7 °C for pure CH_4 hydrate), the observed dissociation was a combination of localized heating and N_2 injection. A flow test was then initiated to probe whether the newly obtained injectivity could be sustained. A mixture of 60 mol% N_2 and 40 mol% CO_2 was injected with constant volumetric rate of 4 mL/h for 25 h, without any reduction in injectivity.

(a)

(b)

Figure 7. (**a**) Pressure gradient (squares) during N_2 injection into a sandstone core (14.96 cm length) saturated with 0.61 (frac.) of CH_4 hydrate, 0.21 (frac.) of water, and 0.18 (frac.) of CH_4 gas. The temperature (circles) was measured on the surface of the core-end at the inlet side. (**b**) Thermal stimulation of a plugged core during constant pressure injection of N_2 at 93 bar. After the injectivity was resumed, a mixture of 60 mol% N_2 and 40 mol% CO_2 was successfully injected for 25 h. Theoretical equilibrium temperature for CH_4 hydrate is approximately 9.7 °C (at 83 bar pore pressure). The temperature was measured on the surface of the core-end at the inlet side.

4. Discussion and Field Implications

The experimental results demonstrated that CO_2 hydrates consistently formed solid flow barriers in high-permeable sandstone core samples for a range of injection rates. The tortuous pore network facilitated hydrate nucleation at CO_2-water interfaces and from CO_2 dissolved in water. Growth of sedimentary CO_2 hydrates in the near-well region and reduced injectivity may lead to technical challenges and higher costs. We emphasize that the presented results are based on microfluidic

and core-scale observations with confined fluid flow, and are not directly comparable to field scale, e.g., in terms of fluid contact areas, cross-sectional flow, and rate of heat transfer. The experimental data can, however, contribute to improved physical understanding and simulation validation of thermodynamic and transient flow models.

From the presented experiments (Figures 2 and 5), N_2 failed (40 mL injected), whereas MeOH succeeded (25 mL injected), in contacting and dissociating the CO_2 hydrates obstructing fluid flow in the core samples. The destabilization mechanisms behind the inhibitors are not identical; MeOH lowers the water activity and interacts with the water cages in the hydrate structure, whereas N_2 dilutes and interacts with the hydrate guest molecule (shielded by a water cage) and hydrate subsequently dissociates toward the gas phase where the chemical potential is lower. Hydrate dissociation is an endothermic process that can cause secondary hydrate and ice formation, depending on the rate of heat transfer. Being a freezing-point depressant, MeOH can impede local ice formation associated with hydrate dissociation. The inhibitor lowers the freezing point of ice by approximately the same amount as it lowers the hydrate formation temperature [37]. Furthermore, MeOH is miscible with the residual pore water, and can take advantage of the already existing water network in the sandstone to contact the hydrate plug. In contrast, N_2 introduces a three-phase flow scenario where immiscible N_2 has to establish its own flow channels in the pore space, displacing liquid CO_2 and/or water. This latter flow scenario can greatly affect the relative permeability of the fluid system. While the rock material and total pore volume were similar, the location of the hydrate plug possibly shifted for the different experiments. Thermal stimulation can effectively treat hydrate blockage zones if sufficient heat transfer rates are present (Figures 6 and 7b). However, once thermal stimulation ended and the temperature returned within the GHSZ, secondary hydrate formation occurred with a faster response than primary formation, due to memory effects (Figure 6). Secondary hydrate formation after stimulation was avoided by binary gas injection at a high nitrogen penalty (60 mol% N_2), hampering overall CO_2 storage capacity. At field scale, thermal stimulation is likely to be less effective than the presented core-scale experiments, due to dimension upscaling and limited penetration range of localized heating.

We hypothesize (Figure 8—conceptual model), based on pore- and core-scale experimental observations, that CH_4 hydrate structures can be porous or non-porous depending on the initial water saturation and final hydrate saturation of the system. We expect CO_2 hydrate structures on the other hand to be non-porous, independent of initial saturations, because of the higher solubility achieved in the water phase. In Figure 8, a single pore (100 μm diameter) is initially filled with a gas bubble surrounded by capillary-bound water. Hydrate formation follows the gas-water interface until the gas phase is either encapsulated by porous hydrate (pathway A) or is consumed due to low initial gas saturation or high solubility (pathway B), resulting in a non-porous hydrate structure. Porous hydrate may be gas permeable, and therefore, a higher hydrate surface area is accessible for contact with injected N_2. A saturation threshold for CH_4 hydrate morphology was identified in the range 0.48–0.58 (frac.) hydrate saturation. For CH_4 hydrates above this saturation value (excess water systems), and for CO_2 hydrates in general, the effect of N_2 to destabilize hydrate plugs and restore flow in sandstone was limited. A similar trend is found elsewhere [38,39], where pressure-induced dissociation rates of CH_4 hydrates decreased with increasing hydrate saturation (>0.5 frac.). Destabilization of non-porous hydrate suffered from low mobility of the liberated gas during initial dissociation, and interactions with neighboring pores were obstructed by the remaining hydrate. Therefore, treating non-porous hydrate blockage in hydrophilic porous media (capillary-bound water preserved) by applying a water-miscible inhibitor, e.g., MeOH, where the hydrate structure is destabilized through the water phase is recommended.
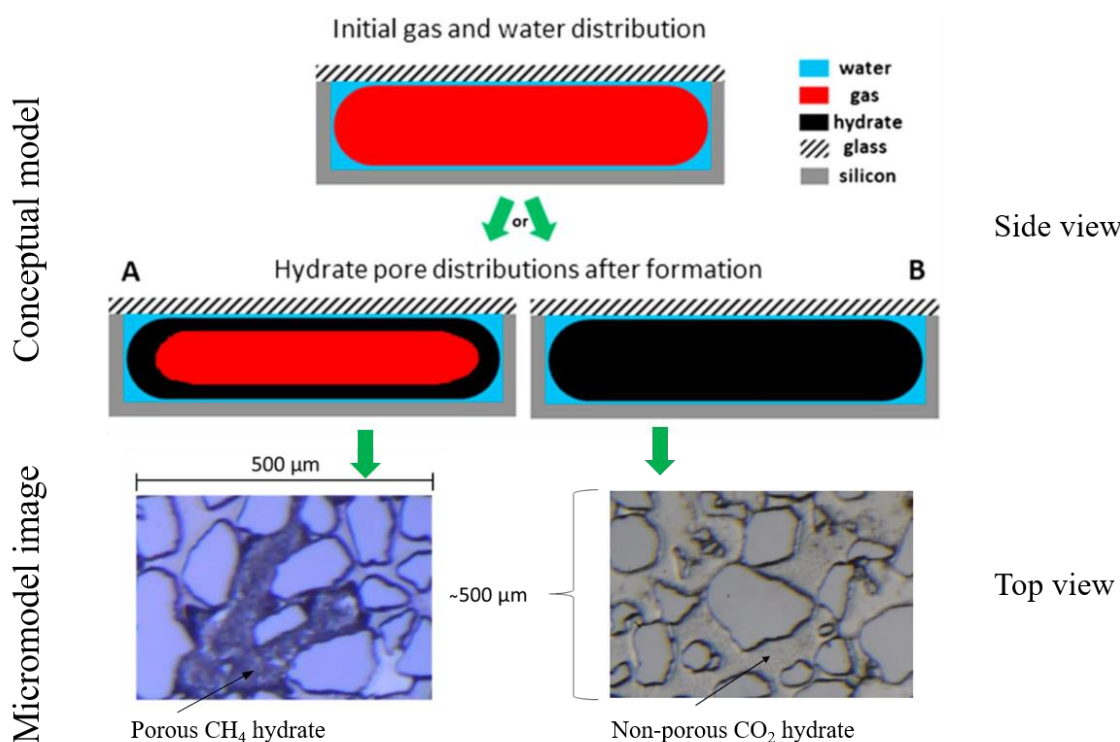
Figure 8. Comparison of porous CH_4 (Type A—left) and non-porous CO_2 (Type B—right) hydrate structures obtained in a hydrophilic, high-pressure micromodel. The hydrate structure formed depended on initial saturations, as well as type of guest molecule. Adapted from [9,38,40].

5. Conclusions

Solid, non-porous hydrate structures formed consistently during CO_2 injection and effectively blocked fluid flow within the pore space in the gas hydrate stability zone (GHSZ). Loss of injectivity due to hydrate barriers in high-permeable sandstones occurred over a range of CO_2 injection rates (0.5–10 mL/min), implying that hydrate formation represents a risk not only during shut-ins and static flow conditions, but also during steady-state fluid flow in sediments. Thermal stimulation and MeOH injection successfully dissolved CO_2 hydrate plugs and restored the formation connectivity, whereas N_2 injection failed to contact and dissociate non-porous hydrate in these experiments. Limitations of using N_2 as a thermodynamic inhibitor were further investigated with CH_4 as a guest molecule at varying fluid saturations. Porous, gas permeable CH_4 hydrates (<0.48 frac. saturation) were successfully dissociated by N_2, whereas non-porous CH_4 hydrates (>0.58 frac. saturation) did not dissociate. In water-wet sediments, MeOH benefited from being miscible with water, and can contact the hydrate zone via preserved water channels. Thermal stimulation proved to be the most efficient remediation method at core scale in near-zero permeability conditions. However, once thermal stimulation ended, and the temperature returned within the GHSZ, secondary hydrate formation occurred with a faster response than primary formation due to memory effects. Determining under which specific conditions the injectivity of a CO_2 source point can be impaired due to unwanted hydrate formation is important to lower the cost and risk barriers associated with carbon geo-sequestration.

Conflicts of Interest: The authors declare no conflict of interest.

References

1. Koide, H.; Tazaki, Y.; Noguchi, Y.; Iijima, M.; Ito, K.; Shindo, Y. Underground storage of carbon dioxide in depleted natural gas reservoirs and in useless aquifers. *Eng. Geol.* **1993**, *34*, 175–179. [CrossRef]
2. IEA. 20 Years of Carbon Capture and Storage—Accelerating Future Deployment. 2016. Available online: https://www.eenews.net/assets/2016/11/15/document_gw_04.pdf (accessed on 30 June 2020).
3. Berntsen, A.; Todorovic, J.; Raphaug, M.; Torsæter, M.; Chavez Panduro, E.A.; Gawel, K. Salt clogging during supercritical CO_2 injection into a downscaled borehole model. *Int. J. Greenh. Gas Control* **2019**, *86*, 201–210. [CrossRef]
4. Hansen, O.; Gilding, D.; Nazarian, B.; Osdal, B.; Ringrose, P.; Kristoffersen, J.-B.; Eiken, O.; Hansen, H. Snøhvit: The History of Injecting and Storing 1 Mt CO2 in the Fluvial Tubåen Fm. *Energy Procedia* **2013**, *37*, 3565–3573. [CrossRef]
5. Eiken, O.; Ringrose, P.; Hermanrud, C.; Nazarian, B.; Torp, T.A.; Høier, L. Lessons learned from 14 years of CCS operations: Sleipner, In Salah and Snøhvit. *Energy Procedia* **2011**, *4*, 5541–5548. [CrossRef]
6. Morozova, D.; Zettlitzer, M.; Let, D.; Würdemann, H. Monitoring of the microbial community composition in deep subsurface saline aquifers during CO_2 storage in Ketzin, Germany. *Energy Procedia* **2011**, *4*, 4362–4370. [CrossRef]
7. Gauteplass, J.; Almenningen, S.; Ersland, G. Storing CO_2 as solid hydrate in shallow aquifers: Electrical resistivity measurements in hydrate-bearing sandstone. *E3S Web Conf.* **2020**, *146*, 05002. [CrossRef]
8. Hoteit, H.; Fahs, M.; Soltanian, R.M. Assessment of CO_2 Injectivity During Sequestration in Depleted Gas Reservoirs. *Geosciences* **2019**, *9*, 199. [CrossRef]
9. Almenningen, S.; Gauteplass, J.; Fotland, P.; Aastveit, G.L.; Barth, T.; Ersland, G. Visualization of hydrate formation during CO_2 storage in water-saturated sandstone. *Int. J. Greenh. Gas Control* **2018**, *79*, 272–278. [CrossRef]
10. Gauteplass, J.; Almenningen, S.; Ersland, G.; Barth, T. Hydrate seal formation during laboratory CO_2 injection in a cold aquifer. *Int. J. Greenh. Gas Control* **2018**, *78*, 21–26. [CrossRef]
11. Awan, A.R.; Teigland, R.; Kleppe, J. A Survey of North Sea Enhanced-Oil-Recovery Projects Initiated During the Years 1975 to 2005. *SPE Reserv. Eval. Eng.* **2008**, *11*, 497–512. [CrossRef]
12. Ding, T.; Liu, Y. Simulations and analysis of hydrate formation during CO_2 injection into cold saline aquifers. *Energy Procedia* **2014**, *63*, 3030–3040. [CrossRef]
13. Kumar, A.; Maini, B.; Bishnoi, P.R.; Clarke, M.; Zatsepina, O.; Srinivasan, S. Experimental determination of permeability in the presence of hydrates and its effect on the dissociation characteristics of gas hydrates in porous media. *J. Pet. Sci. Eng.* **2010**, *70*, 114–122. [CrossRef]
14. Lu, M.; Connell, L.D. Non-isothermal flow of carbon dioxide in injection wells during geological storage. *Int. J. Greenh. Gas Control* **2008**, *2*, 248–258. [CrossRef]
15. Rayward-Smith, W.J.; Woods, A.W. Some implications of cold CO_2 injection into deep saline aquifers. *Geophys. Res. Lett.* **2011**, *38*, 6. [CrossRef]
16. Munkejord, S.T.; Bernstone, C.; Clausen, S.; de Koeijer, G.; Mølnvik, M.J. Combining Thermodynamic and Fluid Flow Modelling for CO_2 Flow Assurance. *Energy Procedia* **2013**, *37*, 2904–2913. [CrossRef]
17. Jamaluddin, A.K.M.; Kalogerakis, N.; Bishnoi, P.R. Hydrate plugging problems in undersea natural gas pipelines under shutdown conditions. *J. Pet. Sci. Eng.* **1991**, *5*, 323–335. [CrossRef]
18. Pruess, K. Numerical simulations show potential for strong nonisothermal effects during fluid leakage from a geologic disposal reservoir for CO_2. In *Dynamics of Fluids and Transport in Fractured Rock*; American Geophysical Union: Washington, DC, USA, 2005; pp. 81–89.
19. Vilarrasa, V.; Silva, O.; Carrera, J.; Olivella, S. Liquid CO_2 injection for geological storage in deep saline aquifers. *Int. J. Greenh. Gas Control* **2013**, *14*, 84–96. [CrossRef]
20. Yang, S.O.; Hamilton, S.; Nixon, R.; De Silva, R. Prevention of Hydrate Formation in Wells Injecting CO_2 into the Saline Aquifer. *SPE Prod. Oper.* **2015**, *30*, 52–59. [CrossRef]
21. Sun, D.; Ripmeester, J.; Englezos, P. Phase Equilibria for the $CO_2/CH_4/N_2/H_2O$ System in the Hydrate Region under Conditions Relevant to Storage of CO_2 in Depleted Natural Gas Reservoirs. *J. Chem. Eng. Data* **2016**, *61*, 4061–4067. [CrossRef]

22. Aspelund, A.; Jordal, K. Gas conditioning—The interface between CO_2 capture and transport. *Int. J. Greenh. Gas Control* **2007**, *1*, 343–354. [CrossRef]

23. Ersland, G.; Husebø, J.; Graue, A.; Baldwin, B.A.; Howard, J.; Stevens, J. Measuring gas hydrate formation and exchange with CO_2 in Bentheim sandstone using MRI tomography. *Chem. Eng. J.* **2010**, *158*, 25–31. [CrossRef]

24. Birkedal, K.A.; Hauge, L.P.; Graue, A.; Ersland, G. Transport Mechanisms for CO_2-CH_4 Exchange and Safe CO_2 Storage in Hydrate-Bearing Sandstone. *Energies* **2015**, *8*, 4073–4095. [CrossRef]

25. Schoderbek, D.; Farrell, H.; Howard, J.; Raterman, K.; Silpngarmlert, S.; Martin, K.; Smith, B.; Klein, P. ConocoPhillips Gas Hydrate Production Test. Final Techinal Report. *USDOE* 2013. [CrossRef]

26. Boswell, R.; Schoderbek, D.; Collett, T.S.; Ohtsuki, S.; White, M.; Anderson, B.J. The Iġnik Sikumi Field Experiment, Alaska North Slope: Design, Operations, and Implications for CO_2–CH_4 Exchange in Gas Hydrate Reservoirs. *Energy Fuels* **2017**, *31*, 140–153. [CrossRef]

27. Zatsepina, O.Y.; Pooladi-Darvish, M. Storage of CO_2 hydrate in shallow gas reservoirs: Pre- and post-injection periods. *Greenh. Gases Sci. Technol.* **2011**, *1*, 223–236. [CrossRef]

28. Panter, J.L.; Ballard, A.L.; Sum, A.K.; Sloan, E.D.; Koh, C.A. Hydrate Plug Dissociation via Nitrogen Purge: Experiments and Modeling. *Energy Fuels* **2011**, *25*, 2572–2578. [CrossRef]

29. Dong, F.; Zang, X.; Li, D.; Fan, S.; Liang, D. Experimental Investigation on Propane Hydrate Dissociation by High Concentration Methanol and Ethylene Glycol Solution Injection. *Energy Fuels* **2009**, *23*, 1563–1567. [CrossRef]

30. Fan, S.; Zhang, Y.; Tian, G.; Liang, D.; Li, D. Natural Gas Hydrate Dissociation by Presence of Ethylene Glycol. *Energy Fuels* **2006**, *20*, 324–326. [CrossRef]

31. Sira, J.H.; Patil, S.L.; Kamath, V.A. Study of Hydrate Dissociation by Methanol and Glycol Injection. In Proceedings of the SPE Annual Technical Conference and Exhibition, New Orleans, LA, USA, 23–26 September 1990; p. 8.

32. Masuda, Y.; Konno, Y.; Hasegawa, T.; Haneda, H.; Ouchi, H.; Kurihara, M. Prediction of methane hydrate dissociation behavior by nitrogen gas injection. In Proceedings of the 6th International Conference on Gas Hydrates (ICGH 2008), Vancouver, BC, Canada, 6–10 July 2008.

33. Clark, L.W.; Frostman, L.M.; Anderson, J. Low Dosage Hydrate Inhibitors (LDHI): Advances in Flow Assurance Technology for Offshore Gas Production Systems. In Proceedings of the International Petroleum Technology Conference, Doha, Qatar, 21–23 November 2005.

34. Ramstad, T.; Rueslåtten, H. *Pore Scale Numerical Analysis for Geological Sequestration of CO_2*; Technical Report; CLIMIT: Oslo, Norway, 2013.

35. Almenningen, S.; Flatlandsmo, J.; Fernø, M.A.; Ersland, G. Multiscale Laboratory Verification of Depressurization for Production of Sedimentary Methane Hydrates. *SPE J.* **2017**, *22*, 138–147. [CrossRef]

36. Circone, S.; Kirby, S.H.; Stern, L.A. Direct Measurement of Methane Hydrate Composition along the Hydrate Equilibrium Boundary. *J. Phys. Chem. B* **2005**, *109*, 9468–9475. [CrossRef]

37. Frostman, L.M.; Przybylinski, J.L. Successful Applications of Anti-agglomerant Hydrate Inhibitors. In Proceedings of the SPE International Symposium on Oilfield Chemistry, Houston, TX, USA, 13–16 February 2001; p. 10.

38. Almenningen, S.; Iden, E.; Fernø, M.A.; Ersland, G. Salinity Effects on Pore-Scale Methane Gas Hydrate Dissociation. *J. Geophys. Res. Solid Earth* **2018**, *123*, 5599–5608. [CrossRef]

39. Almenningen, S.; Fotland, P.; Fernø, M.A.; Ersland, G. An Experimental Investigation of Gas Production Rates During Depressurization of Sedimentary Methane Hydrates. In Proceedings of the SPE Europec Featured at 80th EAGE Conference and Exhibition, Copenhagen, Denmark, 11–14 June 2018; p. 13.

40. Hauge, L.P.; Gauteplass, J.; Høyland, M.D.; Ersland, G.; Kovscek, A.; Fernø, M.A. Pore-level hydrate formation mechanisms using realistic rock structures in high-pressure silicon micromodels. *Int. J. Greenh. Gas Control* **2016**, *53*, 178–186. [CrossRef]